Frictional Drag Mechanisms between Polymer-Bearing Surfaces

T. Kreer,[†] M. H. Müser,*[,†] K. Binder,[†] and J. Klein[‡,§]

Inst. f. Physik, Johannes Gutenberg-Universität, 55099 Mainz, Germany, Department of Materials and Interfaces, Weizmann Institute, Rehovot 76100, Israel, and Physical and Theoretical Chemistry Laboratory, Oxford OX1 3QZ, United Kingdom

Received June 1, 2001. In Final Form: September 17, 2001

The fundamental features of friction between two polymer-bearing surfaces in relative sliding motion are investigated by molecular dynamics simulation. Adsorbed and grafted polymers are considered in good and bad solutions. The solvent is not treated explicitly but indirectly in terms of a Langevin thermostat. In both systems, we observe shear thinning that is attributed to an orientation of the radius of gyration along the sliding direction. This effect is particularly strong for surfaces bearing polymer brushes. In this case, the shear stresses are mainly determined by the degree of the interpenetration of brushes.

I. Introduction

Polymers grafted to or adsorbed on surfaces modify friction forces between these surfaces and thus have important applications as lubricants. Therefore, the investigation of these friction forces between polymer-bearing surfaces has found great attention both experimentally (see e.g. refs 1−12) and via computer simulation (see e.g. refs 13−24). Further motivation to study such systems stems from applications such as adhesion, flow of polymer solutions, and melts through thin extruders and related problems of polymer processing, hydrodynamics of colloids stabilized with grafted polymer layers, dynamics of wetting and spreading phenomena, flotation of minerals and oil recovery, and so forth. In the present study, we focus on the aspects important for nanotribology[25] and are particularly interested in contributing to the understanding of the characteristics in the shear behavior of surfaces with grafted polymers and of surfaces with adsorbed polymers.[3,4,7] In addition, we want to elucidate the effect of solvent quality and thus present a comparative study of several factors that control friction mechanisms between polymer-bearing surfaces and try to use these results for an improved understanding of the pertinent experiments.

Computer simulations of this problem have the distinct advantage that one can prepare absolutely well controlled surfaces; we choose here a rigid perfect face-centered cubic (fcc) crystal surface as substrate, and hence uncontrolled effects such as mesoscopic substrate surface roughness, adsorbed ions or other impurities attached to the surface, and so forth are absent, and the interaction potential between substrate atoms and the monomers of the polymer chain can be chosen at will and is precisely known. Furthermore, our polymer chains are strictly monodisperse. However, computer simulations also have clear disadvantages: due to the complexity of the effective potentials in a chemically realistic, fully atomic description, the accessible time scales would be far too short (on the scale of nanoseconds) and also the length scales too small (a few nanometers) to allow any meaningful conclusion on the present problem, where the length scale of interest is mesoscopic, and time scales of experimental interest can be as large as seconds. Thus, coarse-grained models of polymer chains need to be used, such as the bead−spring model[26] that was used in refs 13, 14, and 16 and is also used here, where each bead represents a group of $n \approx 3-5$ chemical monomers.[27] Even on this coarse-

[†] Johannes Gutenberg-Universität.
[‡] Weizmann Institute.
[§] Physical and Theoretical Chemistry Laboratory.

(1) Klein, J. In *Liquid at Interfaces*; Chrvolin, J., Joanny, J. F., Zinn-Justin, J., Eds.; Elsevier Science: Amsterdam, 1990.
(2) Klein, J.; Peraha, D.; Warburg, S. *Nature* **1991**, *352*, 143.
(3) Klein, J.; Kumacheva, E.; Mahalu, D.; Perahia, D.; Fellers, L. J. *Nature* **1994**, *370*, 634.
(4) Klein, J.; Kumacheva, E.; Perahia, D.; Mahalu, D.; Warburg, S. *Faraday Discuss.* **1994**, *98*, 173.
(5) Granick, S.; Demirel, A. L.; Cai, L. L.; Peanasky, J. *Isr. J. Chem.* **1995**, *35*, 75.
(6) Cai, L. L.; Peanasny, J.; Granick, S. *Trends Polym. Sci.* **1996**, *4*, 47.
(7) Klein, J. *Annu. Rev. Mater. Sci.* **1996**, *26*, 581.
(8) Luengo, G.; Schmitt, F. J.; Hill, R.; Israelachvili, J. *Macromolecules* **1997**, *30*, 2482.
(9) Kilbey, S. M.; Schorr, P.; Tirrell, M. In *Molecular Interactions and Time-Space Organization in Macromolecular Systems*; Morishima, Y., Norisuye, T., Tashiro, K., Eds.; Springer-Verlag: Berlin, 1999.
(10) Baker, S. M.; Smith, G. S.; Anastassopoulus, D. L.; Toprakcioglu, C.; Vradis, A. A.; Bucknall, D. G. *Macromolecules* **2000**, *33*, 1120.
(11) Raviv, U.; Tadmor, R.; Klein, J. A. *J. Phys. Chem. B* **2001**, *105*, 8125.
(12) Tadmor, R.; Janik, J.; Fetters, L. J.; Klein, J. Submitted.
(13) Murat, M.; Grest, G. S. *Phys. Rev. Lett.* **1989**, *63*, 1074.
(14) Thompson, P. A.; Grest, G. S.; Robbins, M. O. *Phys. Rev. Lett.* **1992**, *68*, 3448.
(15) Lai, P.-Y.; Binder, K. *J. Chem. Phys.* **1993**, *98*, 2366.
(16) Grest, G. S.; Murat, M. *Macromolecules* **1993**, *26*, 3108.
(17) Miao, L.; Hong, G.; Zuckermann, M. J. *Macromolecules* **1996**, *29*, 2289.
(18) Grest, G. S. *Phys. Rev. Lett.* **1996**, *76*, 4979.
(19) Lai, P.-Y.; Lai, C.-Y. *Phys. Rev. E* **1996**, *54*, 6958.
(20) Grest, G. S. In *Dynamics in Small Confining Systems III*; Drake, J. M., Klafter, J., Kopelman, R., Eds.; Material Research Society: Pittsburgh, PA, 1997; p 71.
(21) Neelov, I. M.; Borisov, O. V.; Binder, K. *Macromol. Theory Simul.* **1998**, *7*, 141.
(22) Doyle, P. S.; Shafeh, E. S. G.; Gast, A. P. *Macromolecules* **1998**, *31*, 5474.
(23) He, G.; Müser, M. H.; Robbins, M. O. *Science* **1999**, *284*, 1650.
(24) For reviews, see e.g.: Grest, G. S. In *Polymers in Confined Environments*; Granick, S., Ed.; *Advances in Polymer Science 138*; Springer: Berlin, 1999; p 149. Grest, G. S.; Murat, M. In *Monte Carlo and Molecular Dynamics Simulations in Polymer Science*; Binder, K., Ed.; Oxford University Press: New York, 1995; p 476.
(25) *Modern Tribology Handbook*; Bhusahn, B., Ed.; CRC: Boca Raton, FL, 2001.
(26) Kremer, K.; Grest, G. S. *J. Chem. Phys.* **1990**, *92*, 5057.

10.1021/la010807k CCC: $20.00
Published on Web 11/07/2001

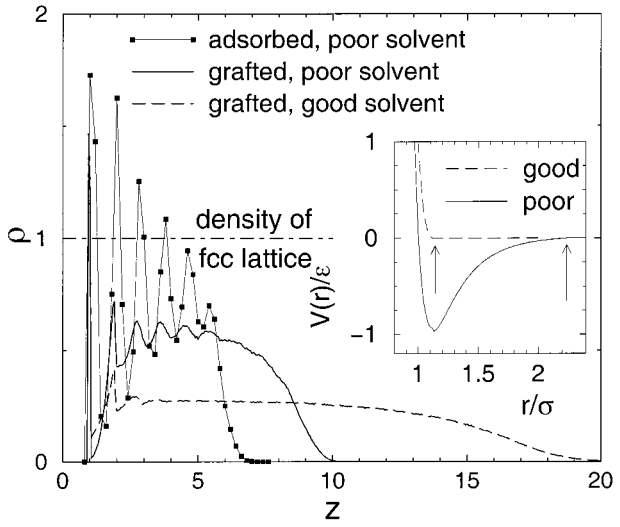

Figure 1. Density profile of uncompressed brushes in the default model ($N = 30, \alpha_s = 0.16/b^2, T = 0.5\epsilon/k_B$). Inset: Effective potential between two unbounded monomers as a function of the solvent quality. The arrows indicate the position where the potentials are cut off.

grained level, one is still constrained to study scales of length and time that are much smaller than those accessed in experiment: Estimating the molecular dynamics time unit roughly with $\tau_{MD} \approx 10^{-11}$ s, the accessible time scales are in the microsecond range, and thus we restrict our attention to polymer chains that are much shorter than the experimental ones, namely, $N = 30$ effective monomers per chain is used in the present work. Our polymers would hence be nonentangled even under melt conditions, unlike the situation encountered in experiments, and while the release of entanglement constraints may be important in the shear response of polymer brushes in the experiments,[7] this relaxation mechanism is clearly not relevant for the present simulations. A further characteristic difference concerns the scales of length and density (Figure 1): the density profile of uncompressed brushes shows density oscillations (this layering phenomenon is a general feature of fluids near hard walls[28]), and the range of oscillations is only a factor of 2 (bad solvent conditions) to 5 (good solvent conditions) smaller than the brush height. Corresponding experiments,[1−12] however, deal with brush heights which are at least an order of magnitude larger, and then the layering or other local structure near the grafting wall cannot even be resolved.[10] Also, the concentration of monomers in the brush stays in the semidilute regime[29] in the experiments, while the simulation (Figure 1) shows densities which correspond to rather concentrated solutions. While in the experiment we thus expect that hydrodynamic interactions play a role for the relaxation mechanism, they are presently screened out under the conditions of the simulations. Thus, we do not even include the solvent molecules explicitly in our simulations, since this saves about an order of magnitude of computing time, and previous work has shown qualitatively similar results[18,24] under conditions of such concentrated polymer solutions.

(27) Binder, K. In *Monte Carlo and Molecular Dynamics Simulations in Polymer Science*; Binder, K., Ed.; Oxford University Press: New York, 1995; p 1.
(28) Israelachvili, J. N. *Intermolecular and Surface Forces*, 2nd ed.; Academic: London, 1991.
(29) de Gennes, P. G. *Scaling Concepts in Polymer Physics*; Cornell University: Ithaca, NY, 1979.

While the simulations thus work in a regime of parameters that complement the regime available to the experiments rather than precisely matching it, the simulations have the distinct advantage that we can change the solvent quality at will, by suitable change of effective interactions between the beads (Figure 1), without any other change of the polymer model or the grafting surface. Moreover, we can also use exactly the same polymer model for the study of adsorbed rather than grafted polymer layers, by simply removing the special bonds between the chain ends and the wall. At the same time, we allow for a weak attraction between the walls and the polymers, while for grafted polymers it is essential that the monomers along the backbone do not adsorb to the substrate. Thus, we are able to perform a comparative study of shear effects on grafted and adsorbed chains and of good solvent versus bad solvent conditions. Despite the large simulation activity,[13−24] no such comparative study has appeared as yet.

In section II, we describe the model in detail and recall its static properties, while section III describes our results for steady-state shear. Section IV presents a discussion and comparison with the experiments, while section V summarizes our conclusions and gives a brief outlook on open problems.

II. Model

To study the fundamental features of friction between two polymer-bearing surfaces in relative sliding motion, a generic model of polymer chains is employed, which has already been used in previous molecular dynamics simulations for similar purposes.[13,18,24] The two walls confining the system consist of parallel [111] planes of an fcc solid. Periodic boundary conditions are imposed in the plane of the walls. The volume region between the walls contains simple bead−spring chains of polymerization N. All particles interact via Lennard-Jones (LJ) potentials

$$V_{LJ}(r_{ij}) = 4\epsilon_{ij}\left[\left(\frac{\sigma_{ij}}{r_{ij}}\right)^{12} - \left(\frac{\sigma_{ij}}{r_{ij}}\right)^{6} - \left(\frac{\sigma_{ij}}{r_{c\,ij}}\right)^{12} + \left(\frac{\sigma_{ij}}{r_{c\,ij}}\right)^{6}\right] \quad (1)$$

r_{ij} is the distance between particles i and j, and $r_{c\,ij}$ denotes the cutoff radius or range of interaction. Note that the choice $r_{c\,ij} = 2^{1/6}\sigma_{ij}$ corresponds to a purely repulsive interaction between the particles. All parameters ϵ_{ij} and σ_{ij} are set to unity, including the mass m of individual monomers, unless mentioned otherwise. The units of energy and length scale will be denoted with ϵ and σ, respectively.

Only atoms within one wall do not interact via LJ potentials. Instead, they are confined to their ideal lattice sites, which are defined relative to the center of mass of the top wall or the bottom wall. The lattice spacing chosen for the confining walls is 1.2σ. The resulting separation of the wall atoms might be considered unrealistically large owing to the large number of atoms in one Kuhn segment even if one keeps in mind the small binding lengths of the C−C bond and the zigzag path along the polymer's backbone. However, one has to remember also that the corrugation of a Kuhn segment is artificially reduced in a coarse-grained model. This leads to distinctly reduced friction (sticking condition) with the wall, in particular in the case of adsorbed monomers. To compensate for this effect in a simple way, we have followed the popular choice for the lattice spacing in the confining walls.

In most of our studies, the top wall is driven externally by imposing a constant velocity, while the bottom wall is always kept fixed. Adjacent monomers in a chain inter-

act with a finitely extensible nonlinear elastic (FENE) potential that acts in addition to LJ potentials:

$$V_{\mathrm{FENE}}(r) = \begin{cases} -0.5kR_0^2 \ln[1 - (r/R_0)^2] & r \le R_0 \\ \infty & r > R_0 \end{cases} \quad (2)$$

where $k = 30\epsilon/\sigma^2$ and $R_0 = 1.5\sigma$. This model, which is widely used in polymer simulations, prevents bond crossing and yields the characteristics of the dynamics of polymer melts.[14,26] The bond length b is defined by the position of the minimum in $V_{\mathrm{FENE}}(r) + V_{\mathrm{LJ}}(r)$. For the present choice of parameters, $b = 0.9945\sigma$. In the following, b will be used frequently to express length scales in order to minimize confusion of the Lennard-Jones σ with the shear stress σ_s.

The focus of this paper is the investigation of the friction mechanism between two sliding polymer brushes in a good solvent. However, bad solvents and adsorbed polymers will be considered as well for comparison. In many simulations of polymers in solution, the solvent is not taken into account explicitly. Instead, the quality of the solvent enters implicitly via the temperature: At large temperatures, the radius of gyration R_g of a chain in dilute solution scales such as $R_g \propto N^{\nu}$ with $\nu \approx 0.59$, which corresponds to the behavior in a good solvent. At low temperatures, one finds $R_g \propto N^{1/3}$, which corresponds to the bad solvent case.[30]

In our simulations, we follow an alternative route to mimic good and bad solvent conditions, because a change of temperature would invoke a change of the gas pressure and thus induce a change in the effective normal load. To keep that pressure constant, all simulations are done at one fixed temperature, namely, $T = 0.5\epsilon/k_B$. To mimic solvent quality, we perform the simulations with two choices of the potential, or to be more precise, with two different values for the cutoff radius r_c of the LJ potential [see eq 1]: (i) $r_c = 2^{1/6}\sigma$. This corresponds to the so-called athermal case in which monomers only repel leading to the scaling of R_g akin to that of the good solvent condition.[16] (ii) $r_c = 2(2^{1/6}\sigma)$. This choice will lead to the scaling $R_g \propto N^{1/3}$, which is reminiscent of the bad solvent case.[30] Figure 1 and Figure 2 might further elucidate the role of the choice for r_c. Note that our temperature of $T = 0.5\epsilon/k_B$ is well below the system's θ-temperature of $T_\theta = 0.7\epsilon/k_B$ for the latter choice of r_c.

Temperature is imposed by a Langevin thermostat. A velocity-dependent friction term and random forces $\Gamma_i(t)$ are added to the equations of motion such that

$$m_i\ddot{\mathbf{r}}_i = -\nabla_i V - \gamma m_i\dot{\mathbf{r}}_i + \Gamma_i(t) \quad (3)$$

where V is the total potential and γ is a viscous damping constant that couples the monomers to a heat bath. Hence, γ plays the role of a viscous monomer−solvent friction. $\Gamma_i(t)$ is a white noise satisfying the fluctuation dissipation theorem:

$$\langle \Gamma_i(t)\Gamma_j(t')\rangle = 6k_B T m_i \gamma \delta_{ij}\delta(t - t') \quad (4)$$

The damping term and the random forces are believed to mimic collisions of monomers with solvent atoms. We will not account for the flow of the solvent into the lower brush. This approximation should be reasonable for very concentrated solutions, where hydrodynamic interactions between the monomers are screened out; see, for example, Figure 2a in ref 22. Instead, the solvent is supposed to be always immobile with respect to the lower surface. Thus, only the top surface is in motion with respect to the solvent. This was meant to mimic the effect of dragging the tip (upper surface) through the solvent. An explicit simulation of the solvent atoms would make the present study computationally unfeasible. Moreover, a realistic flow profile of solvent atoms between two polymer-bearing surfaces in relative sliding motion is not yet known, albeit recently proposed simulation techniques[31,32] suggest promising ways to overcome this shortcoming in a reasonably well controlled way. Note that it is possible to calculate not only the net shear stress on the driven upper wall but also the direct (friction) forces between brushes belonging to the top wall and brushes belonging to the bottom wall. These direct forces do of course depend only very little on the assumptions of the solvent's velocity profile. In our treatment, we certainly overestimate the flow into the upper brush. The main effect is the slightly asymmetric velocity profiles that become apparent in Figure 7 and Figure 11. However, additional simulations were performed with a thermostat where γ was set to zero parallel to the shear direction. None of our conclusions on the direct brush brush interactions have to be altered with such a thermostat.

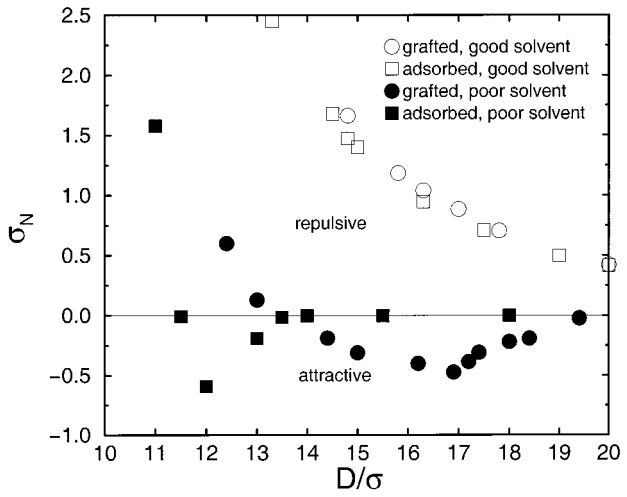

Figure 2. Normal force between polymer-bearing surfaces as a function of surface separation.

Tethering a polymer to a wall is realized by choosing $\epsilon_{hw} = 100\epsilon$ and $r_c = 2(2^{1/6}\sigma)$ between its headgroup and wall atoms. Simultaneously, the mass of the headgroup is increased by a similar factor in order to prevent the system from performing fast oscillations, which would require undesired small time steps Δt. We use here a predictor−corrector algorithm to fifth order and a time step of $\Delta t = 0.005\sqrt{m\sigma^2/\epsilon}$. All other monomers of a grafted chain interact with the wall with $\epsilon_{mw} = 1\epsilon$ and a short-range cutoff $r_{c\,mw} = 2^{1/6}\sigma$. This means that the wall−monomer interaction is purely repulsive. In the case of adsorbed polymers, all monomers are assumed to interact with the wall atoms with $\epsilon_{mw} = 1\epsilon$ and $r_{c\,mw} = 2(2^{1/6}\sigma)$, independent of the solvent's quality. Grafting densities are chosen to be identical on both surfaces. The interactions between monomers are shown in the inset of Figure 1 as a function of the solvent quality.

(30) The relation $R_g \propto N^{1/3}$ has been confirmed for simulations of isolated collapsed chains but is difficult to confirm experimentally, because extremely dilute solutions are necessary to avoid aggregation of the collapsed chains and ultimately polymer−solvent phase separation.

(31) Warren, P. B. *Curr. Opin. Colloid Interface Sci.* **1998**, *3*, 620.
(32) Jendrejack, R. M.; Graham, M. D.; de Pablo, J. J. *J. Chem. Phys.* **2000**, *113*, 2894.

In our simulations, the number of atoms per confining wall is $N_w = 400$. Note that each wall consists of one layer only. Thus, the net number of wall atoms in the two confining walls (layers) is $2N_w = 800$. Our default system furthermore contains 67 polymers with polymerization $N = 30$ grafted to each wall, resulting in a grafting density of $\alpha_g = 0.16b^{-2}$. In simulations of adsorbed polymers, the same total number of polymers is used as in the default system.

All simulations presented in this study for polymer brushes have been carried out in the semidilute regime, which is characterized by a grafting or anchoring density $1 \gg \alpha_g \gg \alpha_g^* \doteq 1/\pi R_{gyr}^2$, where α_g^* denotes the critical grafting density and R_{gyr} is the radius of gyration of an untethered single chain. The default choice of the actually used grafting density of $\alpha_g = 0.16b^{-2}$ (b being the bond length introduced above) satisfies these inequalities sufficiently well for our choice of $N = 30$ ($R_{gyr} \approx \sqrt{N/6}\, b$ for Gaussian chains) and lies well above the critical grafting density of $\alpha_g^* \approx 0.06b^{-2}$. Despite the small degree of polymerization employed in this study, the monomer density of nonoverlapping brushes exhibits the correct characteristics as shown in Figure 1. Similar density profiles for brushes in both good and bad solvent have been reported in experimental[10,33] and computational[13,16,34] studies. We want to note that the plateau in the polymer density in the case of a bad solvent is about 60% of that of a perfectly ordered fcc or hcp (hexagonal close-packed) crystal consisting of nonbonded LJ monomers at the same temperature. The plateau density in the good solvent is 25% of the crystalline reference density. Note that in the experimental brush systems the mean volume fraction of monomers in the unperturbed brush is only ca. 4%. Near the walls, layering effects are observed. These are reflected by density oscillations with adjacent maxima being separated by a distance close to the intramolecular bond length.

The monomer profiles deform considerably in the case of overlapping brushes. Layering is enhanced by decreasing the distance between the surfaces and by decreasing the quality of the solvent. Layering is similar for grafted and adsorbed polymers. The normal forces needed to compress the system are shown in Figure 2. In a good solvent, there are only marginal differences between adsorbed and grafted polymers; however, in the case of a bad solvent significant differences are found. As suggested previously,[35] the attraction between the two surfaces in a bad solvent takes place at considerably larger separation for grafted than for adsorbed polymers.

In this study, we focus on systems that do not exhibit static friction, that is, on brushes that are not too strongly compressed. A simple way to determine whether the system exhibits static friction is to study its free diffusion:[36] A finite system that shows static friction will not diffuse if it is subject to a thermal, fluctuating force like the one defined in eq 3. Instead, it will oscillate around a more or less well-defined equilibrium position. A "viscous" system of finite size as opposed to a solidified system, however, will not appear to be pinned and quickly cross over from the ballistic regime to the diffusive regime; that is, the top wall with the attached brush diffuses as a whole relative to the fixed bottom wall (of course, the diffusion constant for this motion scales inversely in the area of the wall). For wall separations of less than $20b$, only the good solvent case is found to be viscous. As the wall separation decreases to distances of about $14b$, also the good solvent case appears to be pinned. Of course, also "nonviscous" systems become unpinned when the relative velocities of the walls are constrained to nonzero values.

III. Results

In this section, the results for a system under steady shear are presented. The upper wall is moved at a constant velocity $\mathbf{v} = (v, 0, 0)$ while keeping the distance D between the walls constant. We concentrate on the regime $15b \lesssim D \lesssim 20b$, where layering does not (yet) occur near the center of the system. In this regime, the brushes are already significantly compressed with respect to noncontacting surfaces, however, the monomer density is still well below that of an fcc crystal; see Figure 1.

Due to the large dimensionality of our model's parameter space, we mainly confine ourselves to consider the default system ($N = 30$, $D = 17.5$, $\gamma = 2$, $\alpha_g = 0.16$, grafted, good solvent) and compare it to models where typically not more than four of the above-mentioned parameters are varied simultaneously with respect to the default system. In all our simulations, we keep the surface separation D fixed. This often leads to artifacts since a constant normal load is a more natural choice. In our case, however, this is not an issue, because at a given sliding velocity, fluctuations of the calculated instantaneous normal stress on the surface (due to monomer wall interactions) are always small compared to the average normal pressure. This means that for *steady-state* sliding the ensembles $D = \text{const}$ and $\sigma_N = \text{const}$ are equivalent. However, there is a small decrease in σ_N at fixed D with large sliding velocities as can be evidenced from Figure 12. Note that the situation would be dramatically different for brushes under oscillatory shear. In this case, normal forces depend sensitively on the applied frequency for a given surface separation[22] and hence the equivalence between constant load and constant separation breaks down.

Usually, each model, as defined by its parameters, is investigated for sliding velocities $0.01 \le v \le 0.35$. v is given in LJ units [$\sqrt{\epsilon/m}$]. LJ units that would be representative of hydrocarbons are[26] $\epsilon \sim 30$ meV $\approx 400\ k_B K$, $\sigma \sim 0.5$ nm, and LJ time unit $t_0 \sim 3$ ps. At this point, we have to stress that these are very rough estimates that may depend sensitively on temperature, stiffness of the chain, and other details.[37] One should also interpret t_0 *not* as a relaxation time of a polymer but merely as a rough estimate of short-scale motion. Relaxation times of the chains are orders of magnitudes larger than t_0, that is, by at least a factor of the squared degree of polymerization in the unentangled regime.[38]

Note that the large gap between high relative sliding velocities in the simulations and slow velocities in the experiments is partially bridged by the fact that the relevant time scales (relaxation times of polymers) are significantly larger in the experiments than in the simulations. The discrepancy in time scales is due to the larger degree of polymerization in the experiments as compared to the simulations.

(33) Tounton, H. J.; Toprakcioglu, C.; Fetters, L. J.; Klein, J. *Nature (London)* **1988**, *332*, 712.
(34) Wittmer, J.; Johner, A.; Joanny, J. F.; Binder, K. *J. Chem. Phys.* **1994**, *101*, 4379.
(35) Klein, J. *Pure Appl. Chem.* **1992**, *64*, 1577.
(36) Müser, M. H.; Robbins, M. O. *Phys. Rev. B* **2000**, *61*, 2335.
(37) Baschnagel, J., et al. *Adv. Polym. Sci.* **2000**, *152*, 41.
(38) Binder, K.; Lai, P.-Y.; Wittmer, J. *Faraday Discuss.* **1994**, *98*, 97.

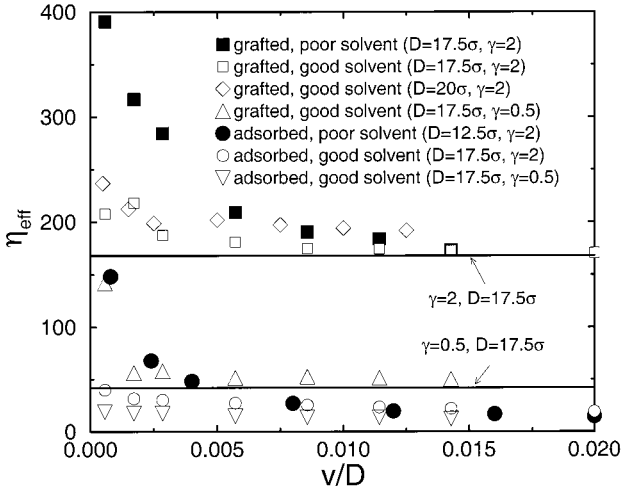

Figure 3. Effective viscosity η_{eff} for adsorbed and grafted polymers in good and bad solutions of varying viscosity as a function velocity v. The solid line represents the response of an uncompressed brush that is dragged through the solvent with $\gamma = 2$.

The quantity of interest is the shear stress σ_s or the effective viscosity η_{eff} which are related via[39]

$$\eta_{\text{eff}} = D\sigma_s/v \tag{5}$$

The shear stress is calculated by adding all forces from the monomers acting on the wall and dividing the result by the area of the wall. We do not intend to anticipate that the shear force gradient is uniform across the gap of width D and that η_{eff} corresponds to a real fluid viscosity. Such an interpretation would be meaningless in the case of shear forces between brushes. At this point, η_{eff} is only introduced in order to represent the drag forces in such a way that the trends for both the low-velocity regime and the high-velocity regime are represented within one plot. Some representative results for η_{eff} are shown in Figure 3. Our results are in good qualitative agreement with refs 13 and 16, where the shear stress is shown as a function of the shear rate. We have chosen η_{eff} as the ordinate because this shows more clearly the deviation of the shear forces from linear response which is obtained in the limit $v \to 0$. A precise determination of the visco(elastic) response in that limit is difficult, because the simulations with small v are very CPU time expensive. Moreover, the application of the fluctuation−dissipation theorem from the equilibrium behavior at $v = 0$ is not trivial either, owing to the large relaxation times of the polymers. A quantitative comparison of our data with those in refs 13 and 16 is not possible, because not all the relevant parameters are known to us. The main trend, namely, shear thinning with increasing sliding velocity, is the same and even a bump similar to the one shown in Figure 3 for the grafted, good solvent case (e.g., $D = 17.5\ b$, $\gamma = 2$) could be found in the data of ref 16. This could be seen after scanning in the data from refs 13 and 16 and plotting it in the way in which we present the data here. For large velocities and grafted chains, the effective viscosity (or the shear stress) is dominated by the interactions of the brushes with the solvent. This is due to the fact that half of all polymers, namely, those grafted to the top wall, are dragged with the average velocity v through the solvent while the other half has velocity zero since the solvent is immobilized with respect to the lower surface and the lower brush. Thus, the mean monomer velocity is half of the upper wall's velocity, $\langle v_m \rangle = v/2$. The velocity profile is different from that of adsorbed polymers, which have a different nonlinear velocity profile leading to $\langle v_m \rangle \leq v/2$. Since polymer chains are not permanently fixed at the top wall, monomers adsorbed at the top wall may get detached and readsorbed at other surface sites later, so that the average velocity of the chains adsorbed to the top wall is less than the wall velocity itself.

For both adsorbed and grafted polymers, we find shear thinning; for example, η_{eff} decreases with increasing shear rate, which agrees with previous simulations on hexamers between weakly adsorbing surfaces[40] and simulations[18] and experiments[7] of polymer brushes between surfaces. To deepen our understanding of the shear stress between polymer-bearing surfaces, we will study the effect of various parameters on the effective viscosity. Adsorbed and grafted polymers will be treated separately.

A. Adsorbed Polymers. Before discussing the results for adsorbed polymers under shear, we will briefly discuss the Navier−Stokes equation for our system. To do this, we assume a constant viscosity of the polymers η_{bulk} throughout the film, which is supposed to be identical with the bulk's viscosity at small sliding velocities. If we keep in mind the friction term in eq 3 describing the coupling of the monomers with the thermostat, the Navier−Stokes equation reads

$$\eta_{\text{bulk}} \Delta \mathbf{v}_m(z) = \gamma \rho \mathbf{v}_m(z) \tag{6}$$

where ρ is the mass density of the monomers, which is approximately constant throughout the film not too close to the walls, and $\mathbf{v}_m(z)$ is the monomer velocity profile. With the boundary conditions $v_{m\,x}(0) = 0$ and $v_{m\,x}(D) = v_0 \leq v$, the velocity profile is

$$v_{m\,x} = \frac{\sinh(\sqrt{\gamma\rho/\eta_{\text{bulk}}}\,z)}{\sinh(\sqrt{\gamma\rho/\eta_{\text{bulk}}}\,D)}\, v_0 \tag{7}$$

The main part of the shear stress σ_s can be obtained by integration over the dissipated force, namely, the right-hand side of eq 6, resulting in

$$\sigma_s = \gamma \int \mathrm{d}z\, \rho v_m(z) = \sqrt{\frac{\eta_{\text{bulk}}}{\gamma\rho}}\, \frac{\cosh\left(\sqrt{\frac{\gamma\rho}{\eta_{\text{bulk}}}}\,D\right) - 1}{\sinh\sqrt{\frac{\gamma\rho}{\eta_{\text{bulk}}}}\,D}\, v_0 \tag{8}$$

In the limit of large wall separation $D \gg \sqrt{\eta_{\text{bulk}}/\gamma\rho}$, this can be approximated to

$$\sigma_s \approx v_0 \sqrt{\eta_{\text{bulk}}\gamma\rho} \tag{9}$$

Note that the ratio v_0/v depends on the stick condition of the adsorbed monomers. At large wall velocity v and large damping γ, one can expect less stick than at small v and small γ, respectively. Of course, the treatment in eqs 6−9 is a quasi-macroscopic one; strictly speaking, it is appropriate only for length scales that are large in comparison to the length scale over which the layering of the density occurs (Figure 1).

(39) Happel, J.; Brenner, H. *Low Reynolds Number Hydrodynamics*; Prentice Hall: Englewood Cliffs, NJ, 1965.

(40) Manias, E.; Bitsanis, I.; Hadziioannou, G.; ten Brinke, G. *Europhys. Lett.* **1996**, *33*, 371.

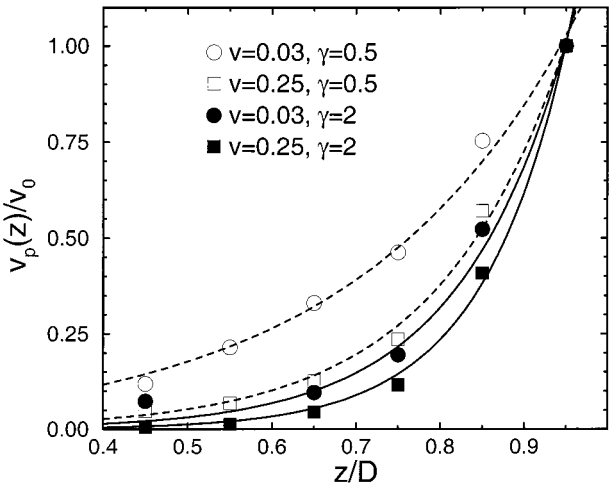

Figure 4. Velocity profile of adsorbed chains in good solvent for two shear velocities and solvent viscosities. The velocities are normalized to the mean velocity of the outermost polymer layer. The wall distance is $D = 17.5b$. The lines represent fits according to eq 7.

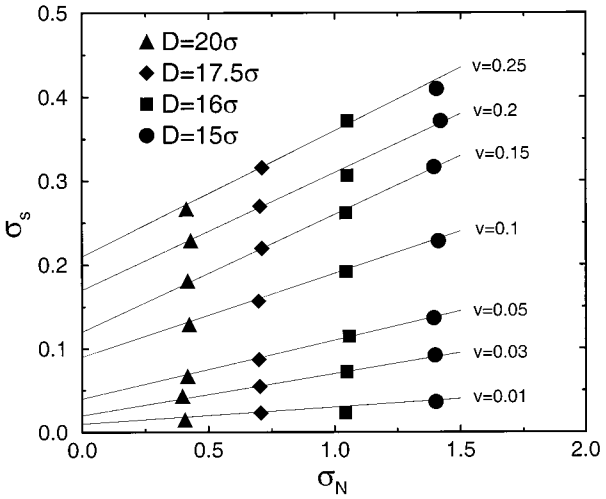

Figure 5. Net shear stress σ_s for adsorbed chains in good solvent with $\gamma = 2$ as a function of σ_N for various shear velocities v and wall distances D. Solid lines are linear fits through the data.

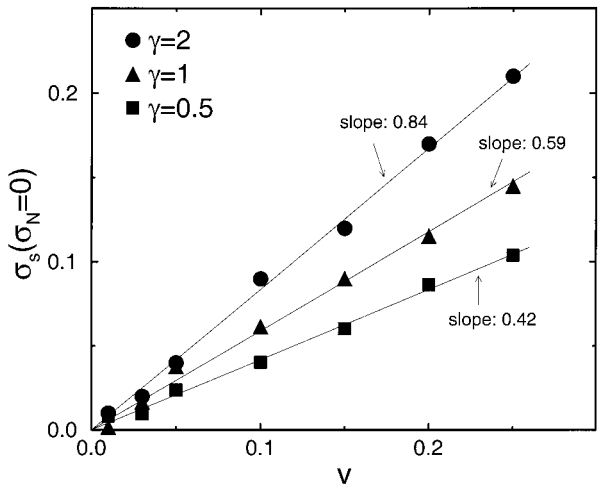

Figure 6. Extrapolation of σ_s from previous figure to zero normal stress as a function of wall velocity v for various couplings γ to solvent.

Some results for the velocity profile of monomers belonging to adsorbed chains are shown in Figure 4. The simple Navier−Stokes equation describes the velocity profile well for small wall velocities v and small coupling to the solvent γ. However, the normalized curves for $\gamma = 0.5$ do not collapse for the two velocities $v = 0.03$ and $v = 0.25$. As we will discuss later, the large velocity gradient near the upper wall in the $v = 0.25$ simulation stretches the polymers along the flow direction. This presumably results in the strongly reduced effective shear viscosity η_{eff} which we have used as a fit parameter in Figure 4. The two curves for $v = 0.03$ on the other hand can be described with a similar value for η_{eff}. For $v = 0.03$, the elongation of the polymers parallel to the upper surface's velocity is much smaller than for $v = 0.25$ (see Figure 10 below).

Of course, for large values of ∇v, deviations from the simple Navier−Stokes equation (eq 6) have to be taken into account in order to reflect strong deviations from thermal equilibrium such as the stretching of the polymers. For small sliding velocities, $v < 0.03$, η_{eff} is relatively independent of γ as long as $\gamma < 2$, indicating that the rheological response is still close to the linear response regime in that case.

Figure 4 furthermore confirms the assumption of a mean monomer velocity (much) smaller than $v/2$ for adsorbed monomers. This explains why our net shear force as shown in terms of an effective viscosity in Figure 3 is smaller for adsorbed polymers than for grafted polymers, which is in contrast to experiment.

For a given sliding velocity, the shear stress turns out to depend linearly on the normal pressure σ_N as can be seen in Figure 5. A linear change in σ_s with σ_N is well-known for two solid bodies in relative motion,[25] and there are relatively simple quasi-geometrical explanations why the *static* friction force between two (boundary lubricated) solids shows this dependency.[41] However, those geometric arguments cannot be applied in a straightforward way to the frictional drag forces investigated in this study.

A possible interpretation of the relation $\partial\sigma_s/\partial\sigma_N \approx$ const can be based on the following scaling argument: Both theory and experiment[42] suggest that in the moderately strong compression regime the interaction energy per unit area $E(D)$ of interacting adsorbed layers in a good solvent is $E(D) \propto D^{-1}$. Thus, the normal shear stress goes as $\sigma_N = -E(D)/D \propto D^{-2}$. The effective viscosity in the overlap region of extent δ, say, of the two interacting adsorbed layers, goes as $\eta_{eff} \propto c \propto D^{-1}$, on the assumption that the polymers are unentangled, where c is the monomer concentration in the gap and is assumed to be uniform across the gap. If we assume that δ is more or less independent of σ_N in the range of Figure 5, then substituting $\eta_{eff} \propto D^{-1}$ in eq 5 gives $\sigma_s \propto D^{-2}$, that is, a linear increase of σ_s with σ_N as in Figure 5. This type of scaling argument should work best for very long chains and semidilute concentrations, conditions which apply to our simulations at best approximately, however.

Also, the extrapolations of the $\sigma_s(\sigma_N)$ curves show an interesting proportionality with the velocity v of the upper wall; see Figure 6. Remember that the bare data (at a given nonzero normal load) show rather nonlinear behavior. Of course, at low load, D is large and hence ∇v is relatively small. This favors the validity of the Navier−Stokes equation and the proportionalities suggested in eq 9. Note that the stick condition $v_0 = v$, which allows replacement of v_0 with v in eq 9, is particularly well

(41) Müser, M. H.; Wenning, L.; Robbins, M. O. *Phys. Rev. Lett.* **2001**, *86*, 1295.
(42) Klein, J.; Luckham, P. *Macromolecules* **1984**, *17*, 1041.

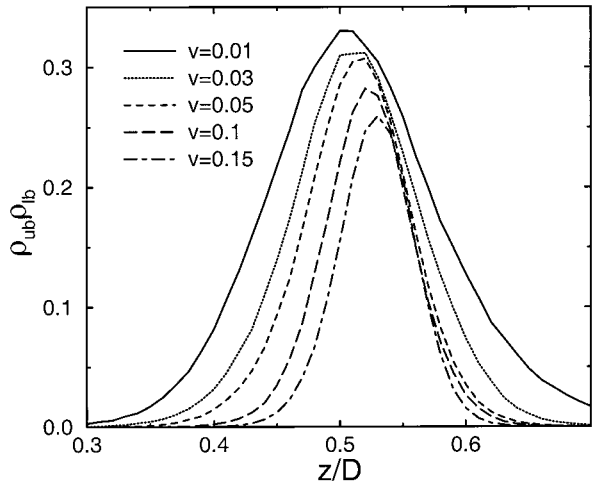

Figure 7. Folded density profile $\rho_{ub}\rho_{1b}$ of polymer brushes in good solvent under different shear velocities ($D = 17.5b$, $\gamma = 2$, $N = 30$, $\alpha_g = 0.16$). ρ_{ub} and ρ_{1b} denote the density of monomers belonging to the upper brush and lower brush, respectively.

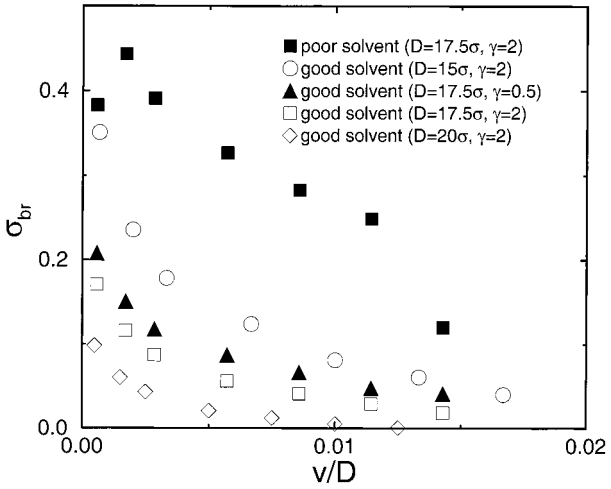

Figure 8. Direct brush−brush shear stress σ_{br} as a function of shear rate for different models.

satisfied at small loads. Of course, stick is also favored by small values of γ and v.

B. Grafted Polymers. The net shear stress σ_s that is measured in the simulations comes from the coupling of the polymers which are grafted to the upper surface to the thermostat which mimics the solvent plus a contribution σ_{br} which comes from the direct brush−brush interaction. This section focuses on the latter contribution σ_{br}. It is calculated by adding up all forces between monomers "belonging" to different walls (via their chemical bonds) and dividing the sum by the area of contact. A key quantity to understand σ_{br} certainly is the overlap of the brushes from opposite sides of the interface. While it is difficult to measure the overlap between the brushes experimentally, this quantity is easily accessible in computer simulations. In Figure 7, the folded density profile is analyzed for our default model for different velocities. The extent of contact between opposing brushes decreases systematically with increasing velocity v. This explains why the net brush−brush friction decreases with increasing sliding velocity; see Figure 8 for some representative graphs. The decrease of σ_{br} with v shown in Figure 8 for the good solvent case can be reasonably well described with a logarithmic velocity dependence.

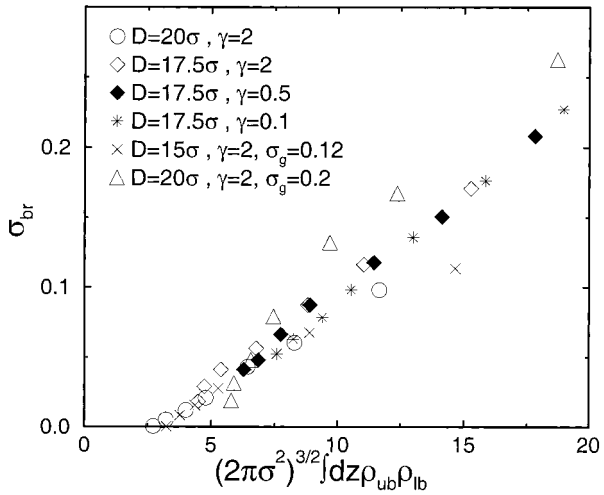

Figure 9. Direct brush−brush shear stress σ_s for different models at various sliding velocities as a function of the overlap integral. Large velocities correspond to small direct brush−brush interactions and vice versa.

To analyze the dependence of σ_{br} on the overlap, we first show that the integral over the overlap is closely related to the number of interactions that take place between monomers belonging to the lower surface and those belonging to the upper surface. The number of interactions per unit area N_{int}/A can be estimated with

$$N_{int}/A \propto \frac{1}{A}\sum_{i(ub)}\sum_{j(1b)} \exp\{-(\mathbf{r}_i - \mathbf{r}_j)^2/2\sigma^2\} \qquad (10)$$

where the sums over monomers with index i and j only include upper brush and lower brush monomers, respectively. Assuming that the density profile only varies on length scales that are large compared to the atomistic dimension σ or b, the right-hand side of eq 10 can be written as

$$I_o = (2\pi\sigma^2)^{3/2}\int dz\ \rho_{ub}(z)\ \rho_{lb}(z) \qquad (11)$$

within the mean-field assumption $\rho_{ub}(\mathbf{r}) \approx \rho_{ub}(z)$. We have explicitly checked the linearity between N_{int}/A and the overlap integral I_o for many different parameter sets. A proportionality constant larger than but in the order of unity was found. The proportionality constant does, however, depend slightly on the grafting density and the wall separation.

In Figure 9, the net brush−brush interactions σ_{br} are plotted versus the overlap integral I_o for a large variety of model parameters. It can be seen that the value of σ_{br} is mainly determined by the overlap I_o.

Velocity effects seem to be implicitly included in I_o, which might appear counterintuitive at first sight. If two configurations have the same amount of overlap but different sliding velocities, we would expect the fast sliding system to show larger friction than the slow sliding system. However, we have to keep in mind that the velocity gradient at the fast sliding interface is much larger than at the slow sliding interface. From the simulations of friction between surfaces bearing adsorbed polymers, we have learned that the effective viscosity decreases with increasing velocity gradient, because the polymers orient along the sliding direction. For grafted polymers, this orienting process is even enhanced due to the flow of the solvent past the brushes; thus, the decrease in the effective

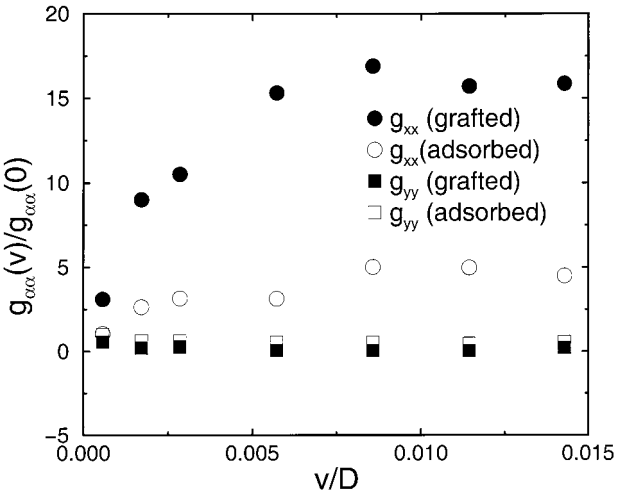

Figure 10. Diagonal elements of the tensor of gyration $g_{\alpha\alpha}$ for adsorbed and grafted polymers as a function of shear rate in good solvent ($D = 17.5b$, $\gamma = 2$). The quantities are normalized by their equilibrium values at $v = 0$.

viscosity is even stronger for brushes than for adsorbed polymers. To summarize, the effect on friction due to an increase in v at a given overlap of the brushes is compensated by a decrease in the effective viscosity.

The effect of sliding velocity on the orientation of the polymers can be seen in the tensor of gyration, which is shown in Figure 10. The tensor of gyration $g_{\alpha\beta}$ is defined as

$$g_{\alpha\beta} = \langle [\sum_{i}^{N} (R_{i\alpha} - \langle R_\alpha \rangle)][\sum_{i}^{N} (R_{i\beta} - \langle R_\beta \rangle)] \rangle \qquad (12)$$

As mentioned in the above paragraph, the orientation effect of the polymers along the sliding direction is much larger for grafted polymers than for adsorbed polymers. It is instructive to represent the tilting effect of grafted polymers by showing snapshots of the simulation. This is done in Figure 11. One can clearly observe the tilting of the polymers and a reduction of the interpenetration by comparing the snapshot for different sliding velocities. Tilting and subsequent reduction in the effective viscosity were also observed for a strongly compressed brush that moved laterally with respect to a flat confining wall in good solvent conditions.[22]

Also for surfaces bearing polymer brushes a linear relationship between the brush−brush shear stress σ_{br} and normal load per area σ_N is obtained within the regime of loads investigated. The relevant data are shown in Figure 12. From that figure, it is possible to extract (differential) friction coefficients $\mu = \partial\sigma_s/\partial\sigma_N$, which we compare to those obtained from Figure 5. The results are shown in Figure 13. For large velocities, μ decreases significantly with v for grafted polymers, but it increases and eventually levels at a value of about 0.15 for the adsorbed polymers.

One could stress again scaling arguments for a possible interpretation of $\sigma_{br} \propto \sigma_N$. The normal stress between brushes in a good solvent goes as $\sigma_N \propto D^{-9/4}$, or for the shorter brushes one may be closer to $\sigma_N \propto D^{-2}$ (see e.g. eq 14 in ref 10)). What is missing is how I_o varies with σ_N. If we assume the result [see e.g. eq 22b of ref 10] that d (the extent of interpenetration which is roughly proportional to δ) varies very weakly with D, as $\delta \propto D^{-1/3}$, then $\delta \propto \sigma_N^{1/6}$, that is, only a very weak variation. We may also assume, as in the scaling argument above, that for the brushes too $\eta_{eff} \propto c \propto D^{-1}$. We also need to augment eq 5 with the effect of increased interpenetration δ since σ_{br} depends directly on this. This gives $\sigma_{br} \propto \delta\eta_{eff}/D \propto D^{-2}\sigma_N^{1/6} \propto \sigma_N^{57/54}$, which is to a good approximation $\sigma_{br} \propto \sigma_N$ and hence close to the results shown in Figure 12. One has to keep in mind again that this type of scaling argument should work best for very long chains and semidilute concentrations. These conditions apply to our simulations at best approximately, however.

IV. Discussion and Comparison to Experiment

Focusing first on the behavior of sheared polymer brushes in good solvent conditions under moderate compression (e.g., $D/b = 17.5$ in Figure 8, noting from Figure 1 that the height of a single uncompressed brush is about $h/b \approx 15$ so that brushes first overlap at $h \approx 30$ b), we see from a comparison of Figures 2 and 8 that the shear stress typically is an order of magnitude smaller than the normal force. Qualitatively, this is the same effect as seen in the experiments;[3,4,7] however, in the experiments it was possible by increasing D somewhat to obtain shear stresses that are many orders of magnitudes smaller than the normal force. It is not possible to fully reproduce this finding with our simulations for a variety of reasons: (i) for larger D, the two brushes interact rather weakly with each other, and then our neglect of taking the solvent explicitly into account becomes more and more unrealistic; (ii) measuring extremely weak shear forces in a simulation that includes so few polymers in the system (our "default system" has no more than 67 polymers grafted to each wall), we would run into a problem of low statistics; (iii) due to the shortness of our chains ($N = 30$ effective monomers per chain only), already the uncompressed brushes are only weakly stretched, and hence we do not have a wide range of D to our disposal. Choosing D too small, one obtains a pronounced layered structure throughout the polymer film all the way from one wall to the other,[21] and one rather encounters the situation of a dense polymer melt or even a confined polymer glass. This situation does not correspond to the experiment either. Nevertheless, we can vary the degree of interdigitation of the two polymer brushes by varying the shear rate (Figure 7), and we find that the shear stress varies approximately linearly with the overlap integral that measures the interdigitation of the two brushes (Figure 9). This result confirms the interpretation that was proposed for the experiments, and it agrees with the findings from various simulations of somewhat different models.[20,21]

A result which so far lacks experimental check, however, is the behavior of two interacting polymer brushes under bad solvent conditions: for $D/b \approx 17.5$, the shear stress is now much larger than previously (Figure 8), although the two brushes are only hardly compressed (Figure 1 shows that the height of a single uncompressed brush under bad solvent conditions is about $h/b \approx 9$), and one is in a regime where the normal force is attractive rather than repulsive (Figure 2). Presumably, this latter observation presents the clue for this surprising strength of the shear forces: the monomers in the tails of the two brush profiles stick to each other, and overcoming this attraction needs a rather strong shear force.

This consideration already presents a distinct hint that for an understanding of the shear properties of polymer-bearing surfaces the solvent conditions are very important. The simulations match up nicely with experiments of adsorbed chains in poor and theta solvents at different

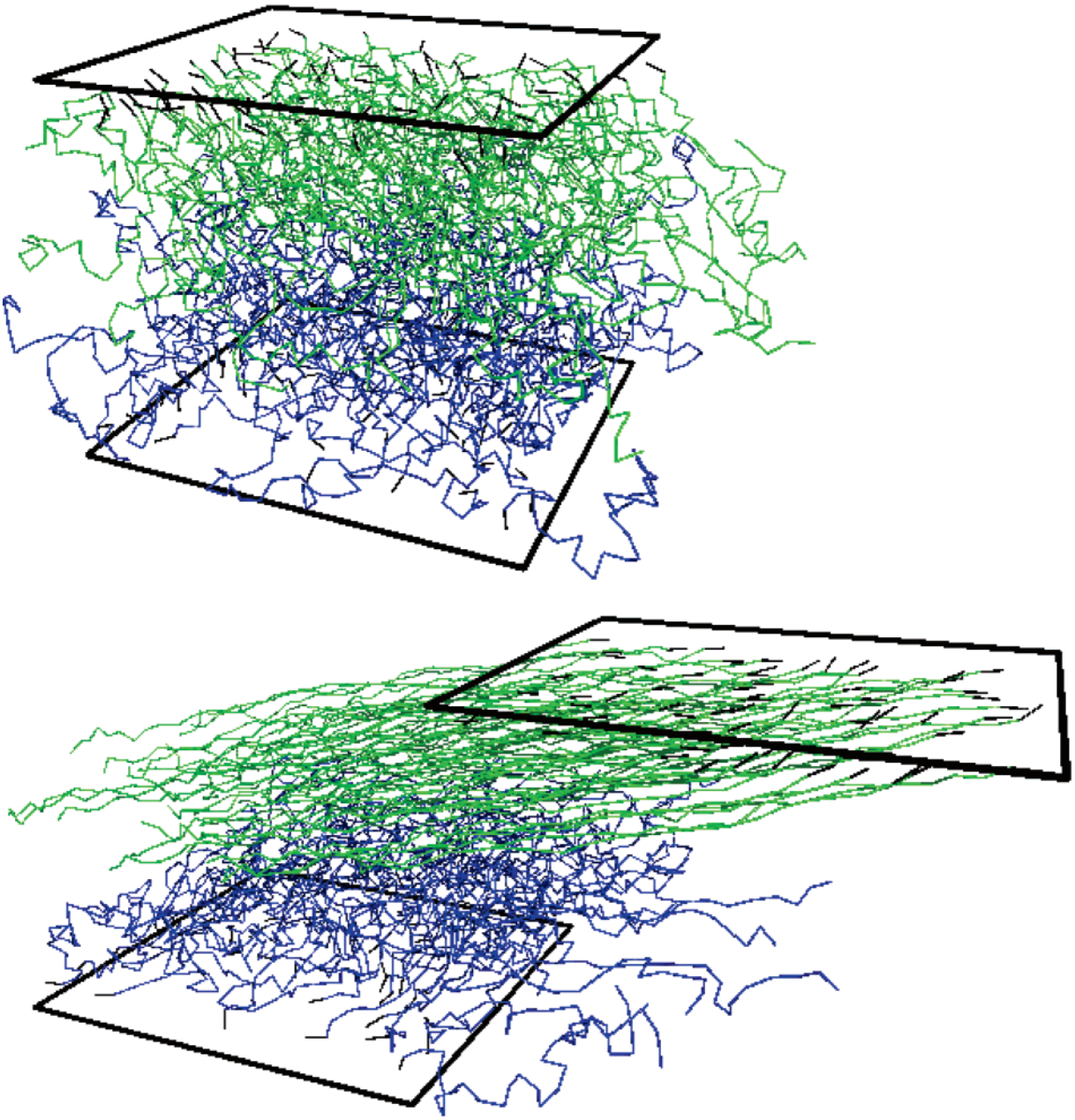

Figure 11. Snapshot of sliding walls bearing endgrafted polymers in good solvent. Polymers grafted to the upper wall are green, and polymers grafted to the lower wall are blue. Periodic boundary conditions are employed. Top: Sliding velocity $v = 0.01$. Bottom: $v = 0.2$.

shear velocities;[4,11] see also Figure 10 in ref 7. Similarly, the simulations roughly match experimental results for grafted chains.[12]

V. Conclusions

We have used computer simulation methods to study the frictional drag experienced by a surface bearing either an adsorbed or a brushlike polymer layer as it slides past a similarly covered surface. For both adsorbed and brushlike layers, we have varied the normal pressure between the surfaces (and thus the intersurface separation), the sliding velocity, and the solvent quality. For the case of adsorbed polymers, our results reveal a rather strong frictional drag in poor solvent conditions (probably due to the monomer−monomer attractions), with a significantly weaker shear force in good solvents. Both results are qualitatively in agreement with experiments. For the case of polymer brushes in good solvents, the most commonly encountered case, we find a remarkable decrease in the frictional drag at higher shear velocities, which is correlated with a corresponding decrease in the extent of overlap and interaction between the opposing brushes. This is due to stretching of the chains as a result of the sliding velocity field and the consequent reduction in the extent of their interaction in the overlap zone. These results too are in qualitative agreement with recent experiments.

Our results suggest several avenues for future simulation work. These include the use of longer chains and studying the effect of chain length and of grafting density for the case of polymer brushes. In particular, this would enable closer correspondence between the simulations and the experiments than is possible at present. Considering much longer chains and keeping the grafting density the

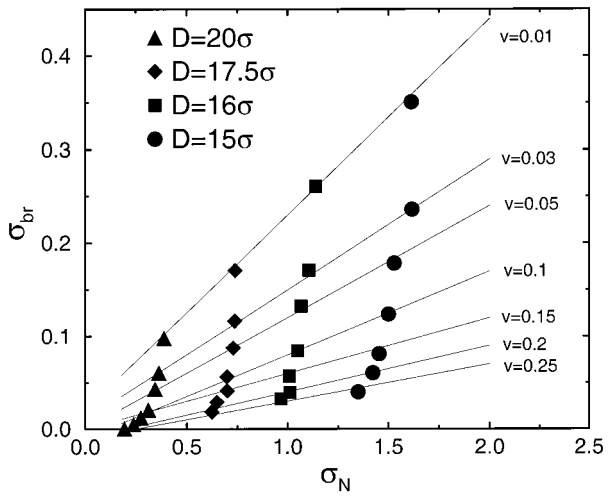

Figure 12. Brush−brush shear stress as a function of normal pressure for different wall separations. Lines are linear fits through the data.

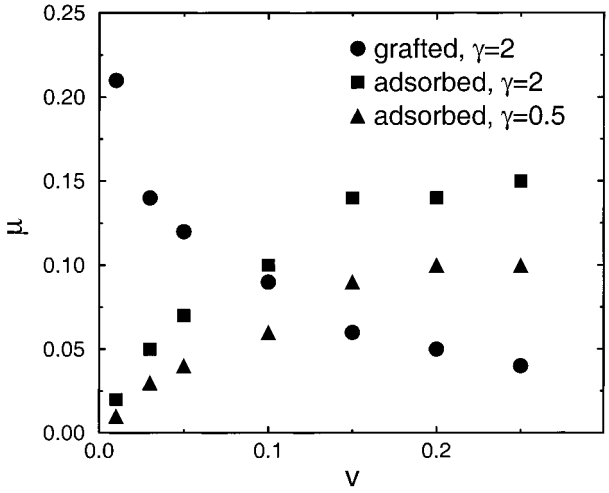

Figure 13. Differential friction coefficient μ for adsorbed and grafted polymers in good solvent as a function of velocity.

same as chosen here is technically very difficult for simulations, however, since then entanglement effects would come into play which lead to a dramatic enhancement of the relaxation times of the grafted chains. However, choosing much longer chains and reducing the grafting density suitably would allow better study of the regime of semidilute concentrations and provide hence a more convincing test of some of the scaling arguments discussed in our paper. Our first results, described in this paper, give us confidence that new and detailed insight into the mechanism of the frictional drag between polymer-bearing surfaces may be obtained from such studies.

Acknowledgment. This research was partially supported by the German−Israeli Project DIP No. 352-101 and by the Bundesministerium für Bildung und Forschung (BMBF) under Grant No. 03N6015. J.K. thanks the Minerva Foundation for partial support.

LA010807K